

Tryptophan scanning mutagenesis reveals distortions in the helical structure of the δ M4 transmembrane domain of the *Torpedo californica* nicotinic acetylcholine receptor

Daniel Caballero-Rivera,¹ Omar A. Cruz-Nieves,¹ Jessica Oyola-Cintrón,¹ David A. Torres-Núñez,² José D. Otero-Cruz³ and José A. Lasalde-Dominicci^{1,3,*}

¹Department of Chemistry; University of Puerto Rico; Rio Piedras Campus; San Juan, Puerto Rico; ²Department of Mathematics; University of Puerto Rico; Rio Piedras Campus; San Juan, Puerto Rico; ³Department of Biology; University of Puerto Rico; Rio Piedras Campus; San Juan, Puerto Rico

Key words: nicotinic acetylcholine receptor, α -bungarotoxin binding, electrophysiology, fourier transform, lipid-exposed transmembrane domains, tryptophan scanning mutagenesis, voltage clamp

Abbreviations: ¹²⁵I-TID, 3-trifluoromethyl-3-(m-[¹²⁵I]iodophenyl) diazirine; ³H-DAF, ³H-diazofluorene; ACh, acetylcholine; α -BgTx, α -bungarotoxin; CBM, caveolin-binding motif; C-R, concentration response; DPPC, dipalmitoylphosphatidylcholine; GluCl, glutamate-gated chloride channel α ; HEPES, N-(2-hydroxyethyl)piperazine-N'-2-ethanesulfonic acid; MENM, mixed elastic network model; nAChR, nicotinic acetylcholine receptor; NMDA, N-methyl-D-aspartate; pLGIC, pentameric ligand-gated ion channel; REFER, rate-equilibrium free energy relationship; SCCMS, slow channel congenital myasthenic syndrome; TMD, transmembrane domain; TrpPP, tryptophan periodicity profile; TrpScanM, tryptophan scanning mutagenesis

The lipid-protein interface is an important domain of the nicotinic acetylcholine receptor (nAChR) that has recently garnered increased relevance. Several studies have made significant advances toward determining the structure and dynamics of the lipid-exposed domains of the nAChR. However, there is still a need to gain insight into the mechanism by which lipid-protein interactions regulate the function and conformational transitions of the nAChR. In this study, we extended the tryptophan scanning mutagenesis (TrpScanM) approach to dissect secondary structure and monitor the conformational changes experienced by the δ M4 transmembrane domain (TMD) of the *Torpedo californica* nAChR, and to identify which positions on this domain are potentially linked to the regulation of ion channel kinetics. The difference in oscillation patterns between the closed- and open-channel states suggests a substantial conformational change along this domain as a consequence of channel activation. Furthermore, TrpScanM revealed distortions along the helical structure of this TMD that are not present on current models of the nAChR. Our results show that a Thr-Pro motif at positions 462–463 markedly bends the helical structure of the TMD, consistent with the recent crystallographic structure of the GluCl Cys-loop receptor which reveals a highly bent TMD4 in each subunit. This Thr-Pro motif acts as a molecular hinge that delineates two gating blocks in the δ M4 TMD. These results suggest a model in which a hinge-bending motion that tilts the helical structure is combined with a spring-like motion during transition between the closed- and open-channel states of the δ M4 TMD.

Introduction

The neuromuscular junction is the synaptic apparatus of the peripheral nervous system (PNS). It is involved in the transmission of the chemical signals that establish communications between neurons and the skeletal muscle. This is achieved by translating the neurotransmitter signal released at the pre-synaptic terminal of nerve endings into a transmembrane ion flux in the post-synaptic muscle fiber.¹ Neurotransmitter receptors are ligand-gated ion channels and one of the best characterized is the nicotinic acetylcholine receptor (nAChR).

The nAChR is an integral membrane protein that belongs to the Cys-loop superfamily of ligand-gated ion channels. Topological studies have revealed that it is composed of four homologous subunits in the stoichiometry of $2\alpha 1:\beta 1:\gamma$ or $\epsilon:\delta$ assembled quasi-pentamerically around a central axis, forming a cation-selective ion channel.^{2,3} Each subunit contains a large hydrophilic extracellular N-terminal domain that bears the ligand binding domains; 4 hydrophobic segments of 19–25 amino acids, denoted as M1–M4, that are proposed to be membrane spanning domains; a large cytoplasmic loop between the M3 and M4 domains that contains phosphorylation sites; and

*Correspondence to: José A. Lasalde-Dominicci; Email: jlasalde@gmail.com
Submitted: 08/07/11; Revised: 01/28/12; Accepted: 01/30/12
<http://dx.doi.org/10.4161/chan.19540>

a short hydrophilic extracellular C terminus.⁴ The M1 and M2 transmembrane domains (TMDs) contribute to the formation of the ion channel pore whereas the M3 and M4 domains, which have the lowest protein sequence conservation across muscle and neuronal nAChR species, form the outer contour and are proposed to have the largest contact with the lipid membrane.⁵

To this date an extremely low number of high-resolution atomic structures of membrane proteins have been acquired due to the complexity of obtaining suitable, well-ordered crystals of these large macromolecules for X-ray crystallography. The X-ray structures of the prokaryotic Cys-loop receptor homologs from *Gloeobacter violaceus* (GLIC)^{6,7} and *Erwinia chrysanthemi* (ELIC)⁸ provided the first high-resolution structural information of members of this superfamily. These two bacterial orthologs share the overall structural features of the Cys-loop superfamily of pentameric ligand-gated ion channels, with ELIC representing a non-conductive state and GLIC representing a conductive state. Recently, the first high-resolution X-ray structure of an eukaryotic Cys-loop receptor, the inhibitory anion-selective glutamate-gated chloride channel α (GluCl) of *Caenorhabditis elegans*, was reported at 3.3 Å resolution.⁹ Currently, the best approximation of the nAChR structure comes from cryo-electron microscopy of the *Torpedo marmorata* nAChR at 4.0 Å resolution (PDB 2BG9), which provides information on the secondary structure and global arrangement of the transmembrane domains.^{3,10} The structure of the soluble acetylcholine-binding protein (AChBP) from *Lymnaea stagnalis*, a structural and functional homolog to the N-terminal extracellular domain of an α 1 subunit, provided insight into the organization of the extracellular domain and revealed the chemical basis for ligand interaction.¹¹ In addition, the crystal structure of the extracellular domain of the nAChR α 1 subunit, while bound to α -bungarotoxin, has been reported at 1.94 Å resolution.¹² However, despite much effort a high-resolution atomic structure of the nAChR has remained elusive to date.

As an important domain of the nAChR that has garnered increasing attention and relevance in the past few years, the lipid-protein interface is composed of the lipid-exposed TMDs and the annular lipid in the immediate perimeter of the receptor. Several studies have made significant advances toward determining the structure and dynamics of the lipid-exposed domains of the nAChR. Studies using photoaffinity labeling,¹³⁻¹⁵ Fourier transform infrared spectroscopy,¹⁶ circular dichroism,¹⁷ two-dimensional ¹H-NMR,¹⁸ and tryptophan scanning mutagenesis¹⁹⁻²⁶ have suggested that the TMDs are organized as helical structures and provided evidence for the dramatic effects of mutations of lipid-exposed domains on the functional states of the nAChR. However, there is still a need to determine how the TMDs move during ACh-induced activation.

In this study, we extend the tryptophan scanning mutagenesis (TrpScanM) approach to dissect the secondary structure and monitor the conformational changes experienced by the δ M4 TMD of the *Torpedo californica* nAChR, and to identify which lipid-exposed positions on this domain are potentially linked to the regulation of ion channel kinetics. This approach has been used successfully for inward rectifier potassium channels,²⁷⁻²⁹ nAChRs,¹⁹⁻²⁶ voltage-activated potassium channels,³⁰⁻³²

glutamate receptors,³³ γ -aminobutyric acid type A (GABA_A) receptors,³⁴ voltage-gated sodium channels,³⁵ *N*-methyl-D-aspartate (NMDA) receptors,³⁶ P2X4 receptors³⁷ and the large conductance mechanosensitive channels (MscL),³⁸ among others. Seventeen residues (Leu-456 to Ile-472) along the δ M4 TMD were systematically substituted for tryptophan and these mutant receptors were characterized by two-electrode voltage clamp and ¹²⁵I-labeled α -bungarotoxin binding assays. Our results show a substantial conformational change (\sim 1.0 amino acid per helical turn) along this domain as a consequence of channel activation, and the difference in oscillation patterns between the closed- and open-channel states suggest a distorted helical structure and the presence of a bending point and a molecular hinge for the δ M4 TMD.

Results

Cell-surface expression levels of the nAChR δ M4 TMD mutants. Seventeen mutations along the core of the *Torpedo californica* nAChR δ M4 TMD (Leu-456 to Ile-472) were successfully engineered by replacing the wild-type (WT) codon for a tryptophan codon at the desired position (Fig. 1A). Analysis of the ¹²⁵I-labeled α -BgTx binding sites revealed different cell-surface nAChR expression levels for the mutations along the δ M4 TMD (Fig. 2 and Table 1). Three mutant receptors (S457W, I460W and L467W) displayed statistically significant increases in nAChR expression levels (2.4-, 2.2- and 2.2-fold increases, respectively) as compared with the WT receptor, suggesting an increase in the efficiency of assembly and/or oligomerization induced by these mutations. Two mutant receptors (P463W and V464W) displayed statistically significant reductions in nAChR expression levels (4.9- and 11.4-fold reduction, respectively), while the remaining 12 mutant receptors (L456W, M458W, F459W, I461W, T462W, M465W, V466W, G468W, T469W, I470W, F471W and I472W) exhibited statistically similar expression levels as the WT receptor. It is noteworthy that the mutations with the lowest nAChR expression levels (P463W and V464W) produced significant increases in functional responses. These results demonstrate that a bulky aromatic side chain can be accommodated at any position along the δ M4 TMD of the *Torpedo californica* nAChR without inhibition of nAChR assembly.

Electrophysiological characterization of the nAChR δ M4 TMD mutants: macroscopic and normalized responses. All 17 mutant receptors were able to elicit ACh-induced currents when characterized by two-electrode voltage clamp (Fig. 1B). Six mutant receptors (M458W, T462W, M465W, V466W, F471W and I472W) displayed statistically significant increases of the maximum macroscopic response (1.3- to 2.0-fold increases) as compared with the WT receptor (Table 1). Three mutant receptors (V464W, T469W and I470W) displayed statistically significant reductions of the maximum macroscopic response (1.5-, 1.7- and 8.6-fold reductions, respectively). The maximum macroscopic responses of the remaining eight mutant receptors (L456W, S457W, F459W, I460W, I461W, P463W, L467W and G468W) were statistically similar to that of the WT receptor. The normalized macroscopic response

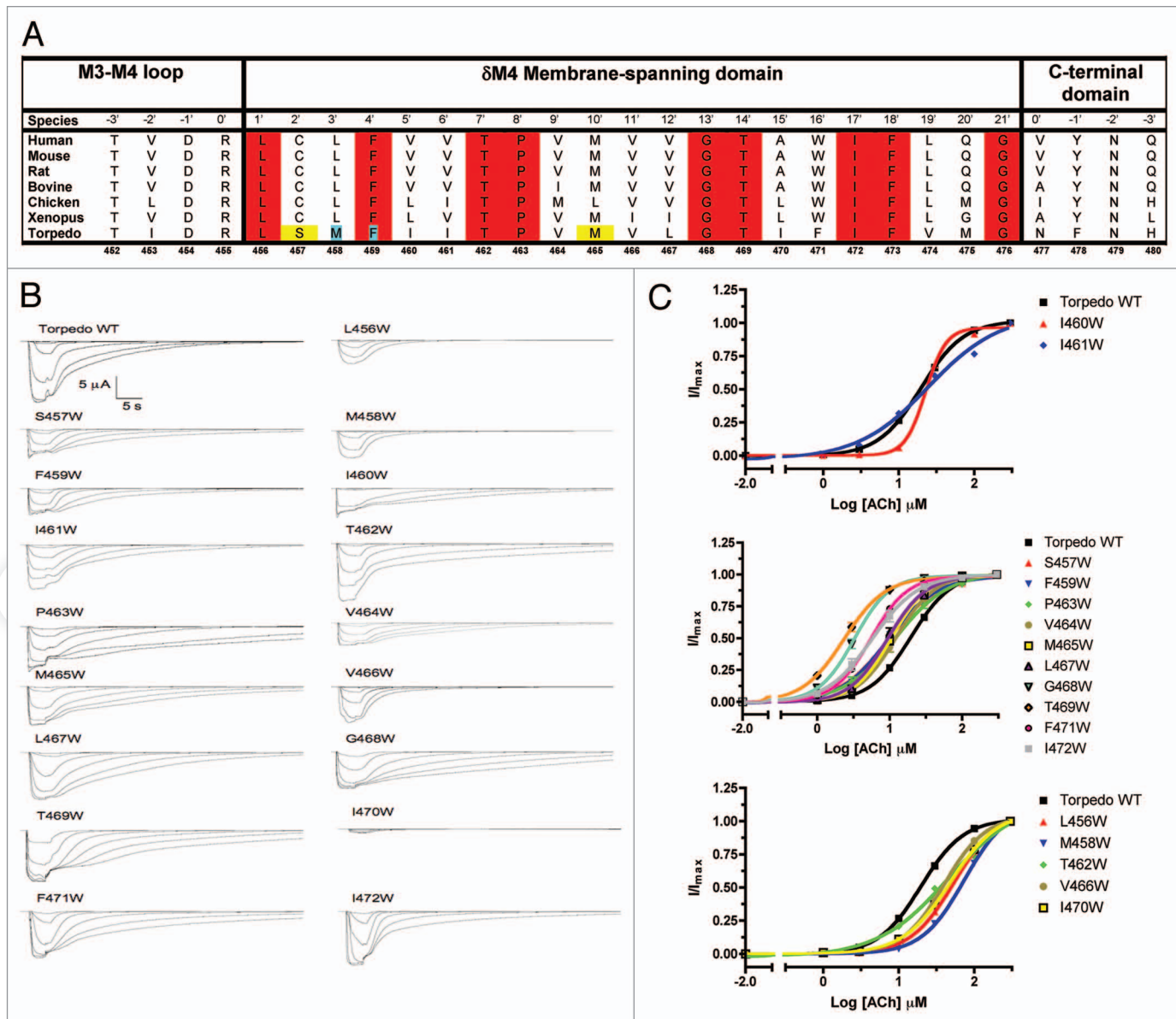


Figure 1. Sequence alignment of the δ M4 transmembrane domain and functional response of wild type and δ M4 mutant nAChRs. (A) Positions Leu-456 to Ile-472 were examined in this study. Positions Ser-457 and Met-465 (highlighted in yellow) were labeled as lipid-exposed using ^{125}I -TID photolabeling affinity.¹⁴ Positions Met-458 and Phe-459 (highlighted in light blue) were labeled with ^3H -DAF photolabeling affinity.¹⁵ Residues highlighted in red are conserved residues among all species. The numbers at the bottom indicate the position in the *Torpedo* δ subunit. (B) Representative families of macroscopic ionic current traces evoked by 1–300 μM ACh and recorded through voltage clamp. Bar scale: 5,000 nA (abscissa), 5 sec (ordinate). (C) Concentration-response curves that were normalized to maximum ionic current for wild type-like (top), gain-of-function (middle) and loss-of-function (bottom) δ M4 mutant nAChRs.

(-nA/fmol) for three mutant receptors (P463W, V464W and V466W) was drastically increased by 5.6-, 7.5- and 4.9-fold, respectively. The normalized macroscopic responses of the remaining 14 mutant receptors were statistically similar to that of the WT nAChR.

Mutant receptors with expression levels similar to the WT nAChR displayed maximum macroscopic responses that were either higher (e.g., F471W) than, lower (e.g., T469W) than or similar (e.g., F459W) to those of the WT nAChR. The three mutant receptors that exhibited higher normalized macroscopic

responses showed either low (P463W and V464W) or WT-like (V466W) expression levels. It is noteworthy that mutant receptors P463W and V464W displayed a dramatic increase in functional response as their EC_{50} values decreased while their normalized macroscopic response increased. However, the V464W mutant displayed a significant reduction in both macroscopic current and expression levels, thus the normalized response was increased. Previous reports from our group have identified mutant receptors with similar behavior in the *Torpedo* α M3, α M4, β M3, β M4, γ M4 and δ M3 TMDs, and the *Mus musculus* α M3 TMD.^{19–21,24–26}

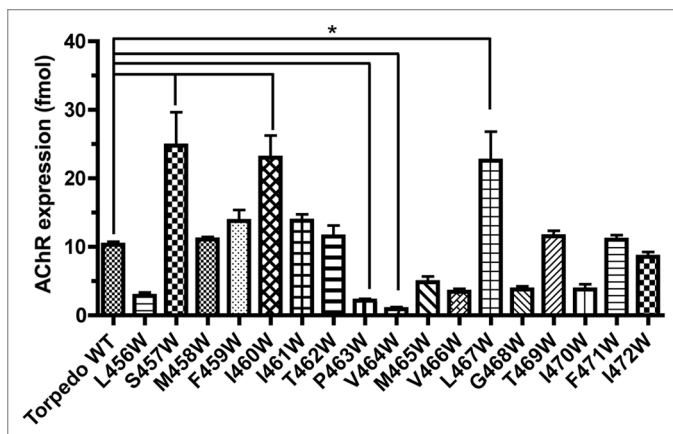


Figure 2. Expression level profile for the δ M4 nAChR mutants. 125 I-labeled α -BgTx binding assays were performed to determine nAChR expression levels in the plasmatic membrane. Each bar represents the mean level of nAChR expression (fmol) \pm SEM * $p < 0.05$ compared with WT nAChR.

These results show that the functional effects caused by the tryptophan substitutions are due to the mutation itself rather than the variation in the nAChR expression levels.

Electrophysiological characterization of the nAChR δ M4 TMD mutants: Potency to ACh and cooperativity. Most of the mutant nAChRs showed typical sigmoidal concentration-response (C-R) curves, with the exception of I461W and T462W that showed steeper curve profiles (Fig. 1C). This would suggest a change in the allosteric properties of these two mutant nAChRs. Five mutant receptors (L456W, M458W, T462W, V466W and I470W) exhibited statistically significant reductions in potency to ACh by 2.0–3.7-fold relative to WT, as evident from the displacement of the C-R curves to higher EC_{50} values (Table 1 and Fig. 1C). In contrast, ten mutant receptors (S457W, F459W, P463W, V464W, M465W, L467W, G468W, T469W, F471W and I472W) displayed a gain-of-function response relative to the WT receptor, as their EC_{50} values were shifted to lower ACh concentrations. In particular, the potency to ACh for the G468W and T469W mutant receptors was enhanced 6.1- and 8.3-fold, respectively. The above results could be due to changes in the affinity and/or efficacy of the agonist. The potency to ACh for each of the other two mutations (I460W and I461W) was statistically similar to that of the WT nAChR, suggesting these residues do not alter the gating mechanism of the nAChR. Several mutations altered the cooperativity of ACh binding to the nAChR as evidenced by changes in the Hill coefficient (nH) of the mutant receptors, relative to the WT (Table 1). All mutant receptors displayed positive cooperativity (nH > 1), with the exception of I461W and T462W that displayed negative cooperativity (nH < 1). The I460W mutant receptor seemed to be in a higher-affinity state as evidenced by the significant increase (1.9-fold) in the Hill coefficient as compared with the WT. In contrast, five mutant receptors (S457W, F459W, I461W, T462W and P463W) appeared to be in a lower-affinity state as compared with WT (1.2–1.7-fold decrease in nH).

Tryptophan periodicity profiles for the open- and closed-channel states. The tryptophan periodicity profile for nAChR expression (fmol/ \AA^3) reveals structural information about the closed-channel state of the δ M4 TMD. 125 I-labeled α -BgTx binding assays were performed in the absence of agonist and with an excess of toxin to assure that all nAChRs on the oocyte surface were bound and completely blocked by the toxin. Furthermore, after α -BgTx incubation oocytes did not display ACh-induced currents at any concentration of the agonist, thus confirming that all nAChRs on the oocyte surface were locked in the closed-channel state conformation. In contrast, the tryptophan periodicity profile produced from the EC_{50} values for ACh activation revealed structural information about the open-channel state of the δ M4 TMD, given that the EC_{50} value estimates the functional state of the nAChR. The tryptophan periodicity profile of the closed-channel state showed an ordered oscillation along most of the δ M4 TMD with a distinctive oscillation pattern between positions Met-458 and Val-464 (Fig. 3A). These diverse oscillation patterns suggest that the δ M4 domain exhibits an irregular helical secondary structure. The distortion of the helix between positions Met-458 and Val-464 could be due to a kink caused by the presence of two consecutive “helix-breaker” amino acids: Thr-462 and Pro-463 (Fig. 1A). A proline in the interior of a helix causes a destabilizing distortion of the helical conformation that introduces a kink in order to avoid a steric clash between the pyrrolidine ring of Pro and the backbone carbonyl group at position *Pro-4*. This bending of the helical structure causes a destabilization of the hydrogen bond network in that region of the secondary structure.^{39,40} A series of overrepresented motifs associating Pro with either Ser or Thr have been identified in helical TMDs and the family of G-protein coupled receptors, with the polar amino acids modulating the deformation of the Pro-kink.⁴¹ The Thr-Pro motif is known to induce an increase in bending angle of the helix compared with a standard Pro-kink, apparently due to the additional hydrogen bond formed between the side chain of Thr and the backbone carbonyl oxygen at position *Thr-4*.^{41,42} Thr-Pro induced kinks in helical TMDs of membrane proteins could have both structural and functional significance since: (1) kinking of the helical structure resulting from backbone rotational restrictions imposed by the Pro psi (ψ) angle can impact the overall TMD structure; and (2) conformational transitions of the protein associated with cis/trans interconversions about the Thr-Pro peptide bond and/or the Pro ψ angle may act as conformational “switches” in the gating mechanism of some ion channels.

The tryptophan periodicity profile of the open-channel state displayed an ordered oscillation along the TMD with small distortions around positions Ile-460, Val-464 and Gly-468 (Fig. 3B). These positions appear as small maximum peaks that seemed to interrupt a well-ordered oscillatory pattern. The distortions around position Val-464 could be caused by the preceding Thr-Pro motif, as explained above, while the distortion around position Gly-468 may be due to the higher conformational flexibility of this amino acid, which tends to disrupt the constrained α -helical structure. The probability of finding a high frequency

Table 1. Biophysical parameters of the torpedo AChR δ M4 TMD mutants

AChR type	EC ₅₀ (μ M)	Hill coefficient	I _{max} (-nA)	¹²⁵ I-Labeled α -BgTx binding sites (fmol)	Normalized response (-nA/fmol)
Torpedo WT	20 \pm 1 (17.24–22.81)	1.58 \pm 0.07	13552 \pm 542	10.3 \pm 0.4	1337 \pm 83
L456W	55 \pm 4* (41.34–68.97)	1.50 \pm 0.05	9293 \pm 859	2.8 \pm 0.5	3673 \pm 458
S457W	9.82 \pm 0.09* (9.526–10.12)	1.23 \pm 0.05*	16226 \pm 750	25 \pm 5*	811 \pm 160
M458W	74 \pm 2* (68.25–80.49)	1.54 \pm 0.03	18178 \pm 591 [§]	11.1 \pm 0.4	1639 \pm 106
F459W	9.8 \pm 0.8* (7.853–11.75)	1.30 \pm 0.05 [§]	16113 \pm 477	14 \pm 2	1044 \pm 99
I460W	22.9 \pm 0.5 (21.40–24.31)	3.08 \pm 0.03*	15052 \pm 515	23 \pm 3*	651 \pm 62
I461W	25 \pm 3 (17.83–32.04)	0.94 \pm 0.02*	16673 \pm 548	13.8 \pm 0.9	1244 \pm 77
T462W	46 \pm 3* (36.75–55.54)	0.92 \pm 0.02*	23826 \pm 1087*	12 \pm 2	2440 \pm 331
P463W	12 \pm 2 [§] (7.552–17.32)	1.3 \pm 0.1 [§]	17028 \pm 1806	2.1 \pm 0.3 [§]	7508 \pm 1207*
V464W	12 \pm 1* (9.345–15.30)	1.62 \pm 0.04	8075 \pm 1528*	0.9 \pm 0.3*	10006 \pm 2718*
M465W	10.7 \pm 0.9* (8.489–12.89)	1.72 \pm 0.02	19981 \pm 628*	4.9 \pm 0.8	4690 \pm 876
V466W	40 \pm 1* (37.28–42.93)	1.57 \pm 0.05	20631 \pm 529*	3.5 \pm 0.4	6491 \pm 784*
L467W	9.5 \pm 0.9* (7.241–11.70)	1.75 \pm 0.01	16790 \pm 460	23 \pm 4*	885 \pm 170
G468W	3.3 \pm 3* (2.646–3.978)	1.76 \pm 0.06	10491 \pm 855	3.8 \pm 0.5	2578 \pm 461
T469W	2.4 \pm 0.2* (1.935–2.858)	1.57 \pm 0.09	8833 \pm 336 [§]	11.5 \pm 0.8	763 \pm 50
I470W	49 \pm 2* (42.61–54.42)	1.39 \pm 0.02	1569 \pm 532*	3.8 \pm 0.8	426 \pm 81
F471W	5.6 \pm 0.3* (4.864–6.358)	1.75 \pm 0.09	27014 \pm 1735*	11.1 \pm 0.7	2550 \pm 225
I472W	6.1 \pm 0.9* (3.656–8.474)	1.48 \pm 0.06	21802 \pm 1761*	8.5 \pm 0.7	2484 \pm 180

All error estimates are expressed as the mean \pm SEM of 5–13 oocytes. Error estimates for EC₅₀ values are also expressed as the 95% confidence interval. *p < 0.01 and [§]0.01 < p < 0.05 compared with response in WT receptor.

of Gly residues at positions *Pro* + 3 to *Pro* + 5 by chance has been estimated to be less than 7%, suggesting that this correlation may reflect modulations of Pro-induced distortions by Gly.³⁹ This profile suggests a kinked helical secondary structure for the open-channel state of the δ M4 TMD.

The periodicity profiles for the δ M4 domain in the closed- and open-channel states illustrated oscillatory patterns of 2.9 \pm 0.5 and 2.0 \pm 0.2 amino acids per helical turn, respectively,

revealing a thinner-elongated helical structure for the open-channel state and a thicker-shrunken helical structure for the closed-channel state (Table S1). The difference in oscillation patterns between the closed- and open-channel states showed a substantial conformational change (\sim 1.0 amino acid per helical turn; p value = 0.0018) along this domain as a consequence of channel activation. These results for the closed- and open-channel states suggest that the helical structure of the *Torpedo*

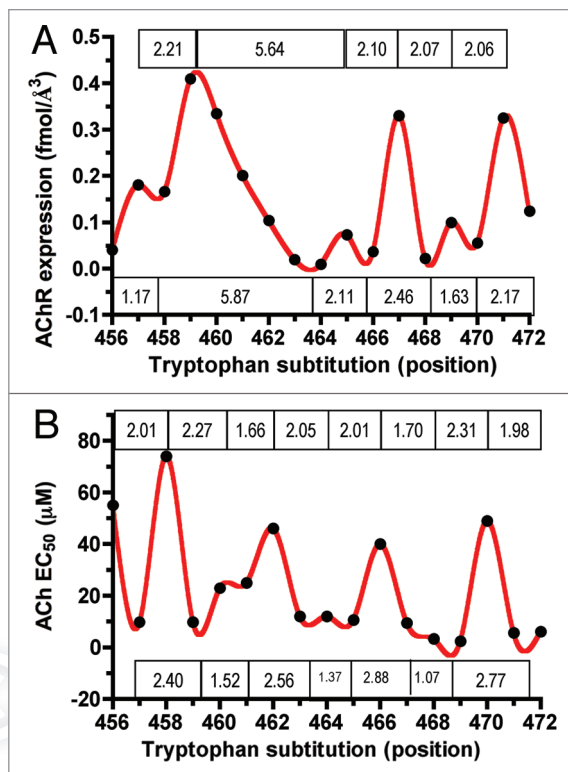


Figure 3. Periodicity profiles for the Torpedo nAChR δ M4 transmembrane domain. (A and B) Tryptophan periodicity profiles for the closed- and open-channel states, respectively. The values inside the boxes indicate the number of residues per helical turn between the adjacent maximums and minimums peaks.

californica nAChR δ M4 TMD displays a spring motion between its different conformational states, similar to the recently proposed spring model for the α M3 TMD of the *Mus musculus* nAChR.²⁴

Helical net diagrams. Helical net diagrams constructed with the tryptophan periodicity profiles for the open- and closed-channel states show that the δ M4 loss-of-function and gain-of-function mutant nAChRs are confined to different ranges of rotation angles (180° region), thus suggesting they are clustered on opposite sides of the helix (Fig. 4). All loss-of-function mutant nAChRs are oriented toward the same face of the helix in both the open- and closed-channel states, suggesting a higher degree of packing within this region of the helix. Most of the gain-of-function mutant nAChRs are oriented toward the opposite side of the helix in the open-channel state, except for the V464W and G468W mutant nAChRs that are found in the region where all the loss-of-function nAChRs are clustered. These apparent outliers correspond to the mutant nAChRs that produce small distortions that seem to interrupt the well-ordered oscillatory pattern of the tryptophan periodicity profiles. Therefore, this discrepancy in the helical net diagrams may be due to the kinks introduced into the helical structure of the δ M4 TMD by “helix-breaker” amino acids near or at these positions. Overall, these results indicate that this domain preserves a helical secondary structure in both the open- and closed-channel states.

Discussion

Functional analysis. In this study we extended the TrpScanM approach to the *Torpedo californica* nAChR δ M4 TMD. Seventeen residues (Leu-456 to Ile-472) along the core of the nAChR δ M4 TMD were periodically substituted for tryptophan and these mutant receptors were characterized by two-electrode voltage clamp and ^{125}I -labeled α -BgTx binding assays. The current structure of the nAChR closed-channel state suggests that positions Ser-457, Met-458, Phe-459, Ile-461, Thr-462, Pro-463, Met-465, Val-466, Thr-469, Ile-470 and Ile-472 are oriented toward the lipid interface.³ Photolabeling affinity experiments using the 3-trifluoromethyl-3-(*m*- ^{125}I iodophenyl)diazirine (^{125}I -TID) and ^3H -diazofluorene (^3H -DAF) probes only identified positions Ser-457, Met-458, Phe-459 and Met-465 on the δ M4 TMD as being oriented toward the lipid interface.^{14,15} The low number of residues labeled as lipid-exposed by this probe is surprising as the M4 domain is predicted to have the largest contact with the lipid membrane. Spatial restrictions at a labeling site can lead to poor labeling efficiency, thus labeling may have been hindered due to distortions and an increased bending angle in the helical structure of the δ M4 TMD, precluding complete or more thorough labeling of the lipid-exposed residues. In addition, the aforementioned probes may have not been able to interact with lipid-exposed residues involved in protein-protein interactions. Position Val-464 seems to be oriented toward the interior of the nAChR in the current structure of the nAChR closed-channel state.³ The reduction in nAChR expression levels caused by a tryptophan substitution at position Val-464 could be due to a steric clash between this tryptophan and residues in the interior of the protein that could affect the stability of the TMD by disrupting the internal hydrogen bond network and the assembly of the multi-subunit protein. In contrast, the reduction in nAChR expression levels observed for the P463W mutant, who according to the structure of the closed-channel state is oriented toward the lipid interface, could be a consequence of a structural destabilization due to disruption of the Thr-Pro motif. However, we hypothesize that this reduction in nAChR expression levels is due to the introduction of a caveolin-binding motif (CBM). A CBM favors partitioning of caveolin-associated proteins into caveolae, a “flask-shaped” subset of lipid raft invaginations in the plasma membrane. Consensus CBMs have been established with the following sequences: $\phi X \phi XXXX \phi$ and $\phi XXXX \phi XXX \phi$; in which ϕ is an aromatic residue (W, F or Y) and X is any amino acid.⁴³ Variations where one to two apolar amino acids (leucine, isoleucine, valine) may substitute the aromatic residues have also been reported in reference 44 and 45. Analysis of the amino acid sequence of the δ M4 TMD reveals that upon a tryptophan substitution at position Pro-463 a CBM is introduced between residues Pro-463 and Phe-471 (WVM VLG TIF). The partitioning of mutant nAChRs into caveolae that is favored by the introduction of the CBM may contribute to the reduced expression levels observed for the P463W mutant nAChR, as is the case for the Torpedo α C418W mutant nAChR.⁴⁶

The increase in nAChR expression levels caused by a tryptophan substitution at position Ser-457 may be due to a favorable

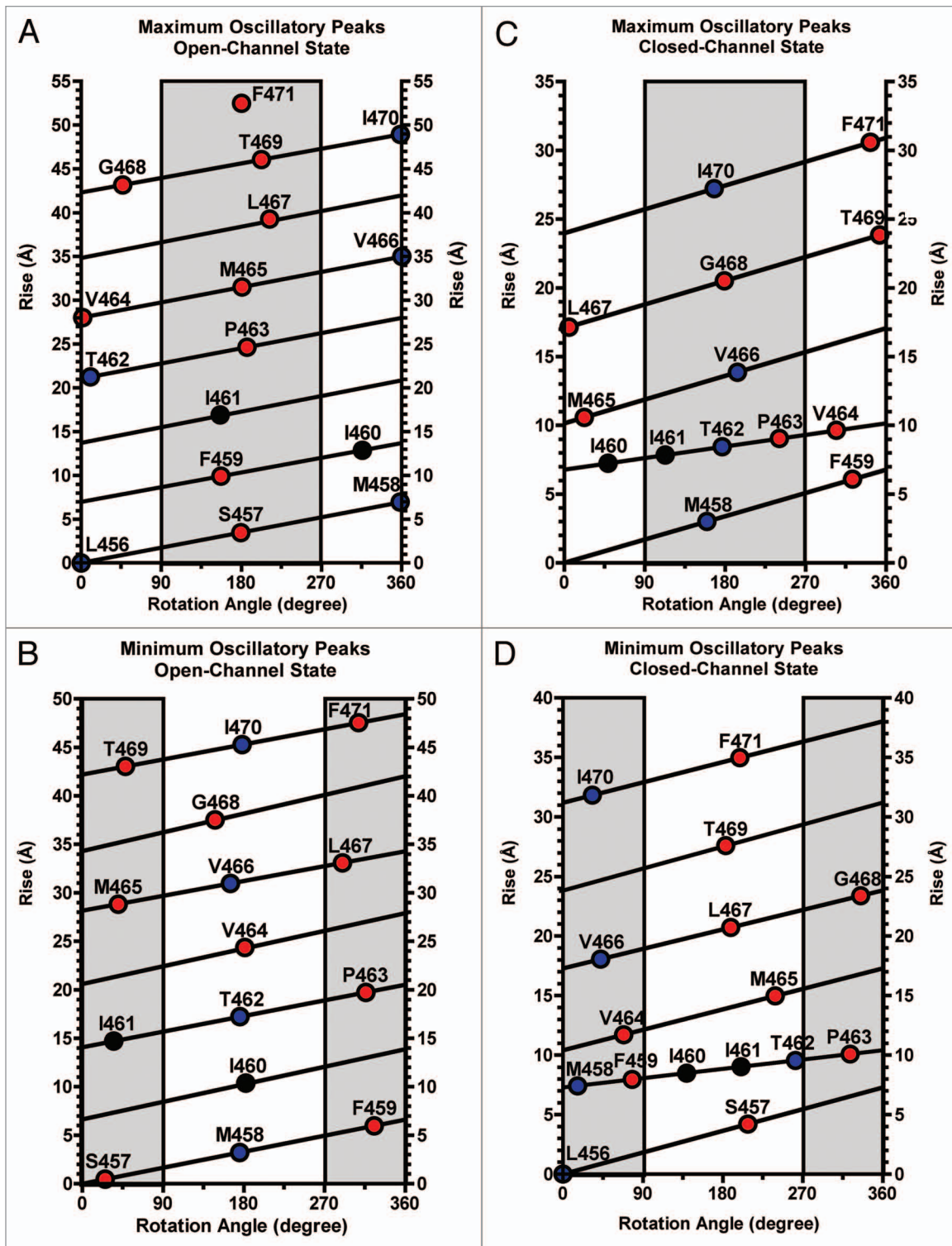


Figure 4. Helical net diagrams for the Torpedo nAChR δ M4 transmembrane domain mutants in the open and closed-channel states. (A–D) Localization and amount of amino acids per helical turn between the adjacent maximum and minimum oscillatory peaks of the periodicity profiles for the Torpedo nAChR δ M4 domain in the open-channel state (A and B) and the closed-channel state (C and D). The gray box delimits the area of the helix where the δ M4 mutants that produced loss-of-function (blue circles) and gain-of-function (red circles) nAChRs are localized based on the data from the tryptophan periodicity profiles.

interaction between the large hydrophobic side chain of Trp and the lipid interface, causing an enhanced assembly of the protein. However, in the current structure of the nAChR closed-channel state positions Ile-460 and Leu-467 are oriented toward crevices facing the M2 and M3 TMDs, respectively.³ These crevices are large enough to accommodate the bulky tryptophan side chain, allowing it to favorably interact with residues on these TMDs and to stabilize the assembly of the multi-subunit protein. Our data was collected from single RNA preparations; therefore, there is a possibility that the changes in ¹²⁵I-labeled α -BgTx binding levels produced by the mutations might reflect alterations in translation efficiency rather than protein stability. However, we believe this to be a remote possibility. In addition, our conclusions are based on the assumption that the multiple biogenesis steps in between translation and folding are invariant in the oocytes. Overall, our results demonstrate that tryptophan can be accommodated at any position along the δ M4 TMD of the *Torpedo californica* nAChR without inhibiting nAChR assembly.

Our results are similar to those previously obtained for the Torpedo γ M4 TMD, in which all tryptophan substitutions produced functional nAChRs, and the α M4 TMD which had only one non-functional nAChR mutant (I417W).^{19,23} In contrast, tryptophan substitutions along the β M4 TMD produced three non-functional nAChRs (L438W, T551W and F455W).²⁵ This finding suggests that the δ M4, γ M4 and α M4 TMDs are less tightly packed than the β M4 TMD. It has been previously demonstrated that a single tryptophan substitution in the lipid-exposed domains can modulate the ion channel function of the nAChR.^{19-26,47-53} Among all mutations, the I470W mutant nAChR showed the most dramatic reduction (8.6-fold) in macroscopic current, but also exhibited a reduction in potency to ACh (higher EC₅₀ value) and expression levels similar to the WT. This suggests an impaired ion channel function for this mutant nAChR that could be due to the lock up of nAChRs in a dysfunctional conformation. In contrast, S457W and L467W displayed significantly higher expression values than the WT and increases in maximum macroscopic currents that were not statistically significant. These results suggest that the increased efficiency in channel assembly and/or oligomerization induced by the tryptophan substitutions at these positions may have also led to a stabilization of the open-channel state of the nAChR and a gain-of-function.

The normalized macroscopic response for three mutant receptors (P463W, V464W and V466W) was drastically increased as compared with WT. Two of these mutant nAChRs, P463W and V464W, exhibited the lowest expression levels of the mutant nAChRs examined. The P463W mutant nAChR also exhibited increases in potency, maximum macroscopic response and normalized macroscopic response. The CBM introduced upon tryptophan substitution at position Pro-463 (**WVM VLG TIF**) is similar to the ones introduced upon tryptophan substitution at positions Cys-418 of the α M4 TMD (**WII GTV SVF**) and Cys-447 of the β M4 TMD (**FVI WSI GTF**), two mutant nAChRs with similar functional characteristics to P463W. Overall, the functional characteristics of the P463W mutant nAChR are similar to the cholesterol-sensitive α C418W mutant nAChR, which is

the first lipid-exposed mutation that has been shown to produce a Slow Channel Congenital Myasthenic Syndrome (SCCMS) in a patient.^{46,54,55} Further studies are underway to determine if the P463W mutant nAChR is cholesterol-sensitive. Taken together, the functional data of the δ M4 mutant nAChRs has demonstrated that this TMD plays an important role in the mechanism of channel gating of the Torpedo nAChR.

Structural analysis. Tryptophan scanning mutagenesis has arisen as a reliable tool to analyze structural-functional patterns in the TMDs of several proteins. In this study, we have applied the TrpScanM approach to identify distortions in helical structure and to monitor the conformational changes experienced by the δ M4 TMD of the *Torpedo californica* nAChR. The open-channel state profile displayed an ordered oscillation along most of the TMD with small distortions that appear as small maximum peaks around positions Ile-460, Val-464 and Gly-468 (**Fig. 3B**). The tryptophan periodicity profile of the closed-channel state showed an ordered oscillation along the portion of the TMD closest to the C-terminal domain (Met-465 to Ile-472) with a distinctive oscillation pattern between positions Met-458 and Val-464 (**Fig. 3A**). These distortions could be due to the kinks introduced into the helical structure of the δ M4 TMD by “helix-breaker” amino acids threonine, proline and glycine near or at these positions.

Analysis of the amino acid sequence of this TMD shows a conserved Thr-Pro motif at positions 462–463, located near the middle of the TMD (**Fig. 1A**), suggesting a bend in the helical structure. The augmented Thr-Pro-kink is also present in the TMD2 of connexin 32⁵⁶ and TMD3 of bacteriorhodopsin,⁵⁷ among other membrane proteins. Specific sequence motifs such as Thr-Pro have been reported to induce distinctive distortions in a TMD by introducing a flexible point,⁵⁸ assisting in helix movements⁵⁹ and/or stabilizing local regions of structural relevance. The structural effects caused by the presence of this motif suggest a wide turn in the TMD that could account for the higher periodicity (5.8 ± 0.1 amino acids per helical turn) observed between positions Met-458 and Val-464 of the periodicity profile of the closed-channel state (**Fig. 3A**), since the Thr in this motif induces a modest increase in the bending angle and a local opening of the helix (altering the twist angle) at the turn preceding Thr.⁶⁰ This segment had a different oscillation pattern in the open-channel state.

The tryptophan periodicity profiles and Fourier transform spectra (see **Sup. Data**) of the δ M4 TMD displayed structural variations between its closed- and open-channel states, as they revealed two different helical structures: a thinner-elongated helical structure for the open-channel state and a thicker-shrunken helical structure for the closed-channel state. The periodicity of the oscillation patterns between the closed- and open-channel states is altered by approximately 1.0 amino acid per helical turn (**Table S1**), suggesting that a substantial conformational change takes place along the δ M4 TMD as a consequence of channel activation. These results suggest that this TMD displays a spring motion when moving between its different conformational states, similar to the recently proposed spring model for the α M3 TMD of the *Mus musculus* nAChR.²⁴ In contrast, the overall helix

movement during channel activation estimated from the tryptophan periodicity profiles of the α M4, β M4 and γ M4 TMDs is more discrete (0.5, 0.4 and 0.3 amino acids per helical turn, respectively), suggesting a more subtle and localized conformational change for these TMDs.^{19,23,25} This can be explained by the fact that the δ M4 TMD is the only M4 TMD that possesses a Thr-Pro or any similar motif that could produce such structural effects. The increase in length by one hydrophobic residue in the open-channel state would extend the helical TMD by 1.5 Å, moving each end closer to the membrane surface.⁶¹ Long helical structures such as the open-channel state of the δ M4 TMD would extend into the aqueous phase if perpendicular to the bilayer, suggesting that it could be tilted in order to bury more of the hydrophobic surface area. In a recent study, mixed elastic network models (MENMs) were developed for the conformational transition between the closed- and open-channel states of two prokaryotic pentameric ligand-gated ion channels (pLGICs).⁶² The MENMs focused on the TMDs, thereby excluding the extracellular domain, but also excluded the M3-M4 loop and the M4 TMD due to gaps in the sequence alignment of the loop connecting M3 and M4 of the two prokaryotic pLGICs. Another MENM included M4 but not the M3-M4 loop. Analysis of the transition trajectories between the closed- and open-channel states identified the tilting motion of some helices in the TMDs, as well as moderate bending and rotation of helices around their own axis.

A recent study monitored the sequence and organization of gating molecular motions in the *Mus musculus* nAChR by measuring diliganded gating equilibrium constants and performing rate-equilibrium free energy relationship (REFER) analysis.⁶³ A change in the gating equilibrium constant following a mutation was interpreted as movement of a residue or its environment between the closed and open conformations. However, a stable gate equilibrium constant does not necessarily imply a lack of movement because the local environment could move along with the residue. In fact, several studies have suggested that some residues in the M4 domains do experience a change in their local environment during the gating mechanism.^{49,52,53,64,65} The sequence of M4 domain motions for the *Mus musculus* nAChR was determined to be α , followed by the ϵ and then the β subunit. The authors suggest that there is no apparent motion in the δ M4 domain because the five characterized mutations in this subunit produced a <6-fold change in the gating equilibrium constant that was not deemed significant. Ten gating blocks have been identified in the nAChR: six in the two α subunits, one in β M4, one in ϵ M4 and two in the δ M2 domain.⁶³ However, REFER analysis was not performed for the δ M4 domain, thus the number of gating blocks for this domain could not be determined.

The tryptophan periodicity profile for the closed-channel state reveals two distinct oscillation patterns flanking the Thr-Pro motif. A comparison between the oscillation patterns of the periodicity profiles of the closed- and open-channel states indicates that the lower half of the TMD (positions 456–464) undergoes greater rearrangements during transition between both states than the upper half (positions 465–472). This suggests that the Thr-Pro motif not only bends the helical structure of the TMD

but that it acts as a molecular hinge that separates (delineates) two gating blocks in the δ M4 TMD. A number of ion channels including the channel-forming peptide alamethicin,⁶⁶ the S6 helix from a voltage-gated potassium channel⁶⁷ and the D5 helix from a voltage-gated chloride channel⁶⁸ contain Pro-induced molecular hinges in their TMDs. Furthermore, a non-proline molecular hinge in the pore-lining α M2 TMD of the nAChR has been implicated in the mechanism of channel gating.^{69,70} Two classes of motion are associated with a proline hinge: swiveling (twisting or rotating around its own axis) and bending (kinking).^{59,71} These distinct hinge dynamics can be combined and one or both types of conformational changes in a TMD could be used to translate a signal across the membrane.⁷¹⁻⁷³ Indeed, voltage-gated K⁺ (Kv) channels sense a change in the transmembrane voltage via a “tilt and twist” motion of their S4 helices.^{74,75}

Recently, a molecular dynamic simulation was used to analyze the conformational dynamics of the nAChR TMDs while embedded in a dipalmitoylphosphatidylcholine (DPPC) bilayer during a 35-ns simulation trajectory⁷⁶ that was based on Unwin's latest structure.³ In this simulation, the gradual tilt away from the Z-axis and the lipid bilayer of the δ M4 TMD indicates that the M4 TMDs increase their hydrophobic interactions with the lipids in the bilayer by burying themselves deeper into the hydrophobic region of the bilayer. The authors observed a partial loss of α -helicity within the TMDs that increased their flexibility inside the lipid bilayer. The bending and turning of the α -helix, coupled with the transition between α -helical characters within the TMD, induced the formation of flexible hinges within the helix, which the authors suggest may be associated with conformational changes of the M2 and M4 TMDs. These results are in agreement with our data.

The localization of several residues in the helical net diagrams suggests a displacement of these residues upon channel activation (Fig. 4A–D). Helical net diagrams constructed with the tryptophan periodicity profiles showed that the δ M4 loss-of-function and gain-of-function mutant nAChRs are confined to different ranges of rotation angles (180° region) in the open- and closed-channel states, thus suggesting they are clustered on opposite sides of the helix (Fig. 4A–D). All loss-of-function mutant nAChRs are oriented toward the same face of the helix in helical net diagrams, suggesting a higher degree of packing within this region of the helix in this state. Most of the gain-of-function mutant nAChRs are oriented toward the opposite side of the helix in the open-channel state, except for the V464W and G468W mutant nAChRs that are found in the region where all the loss-of-function nAChRs are clustered. According to the current structure of the nAChR closed-channel state, mutations that produced a gain-of-function response (i.e., S457W, F459W, P463W, V464W, M465W, L467W, G468W, T469W, F471W and I472W) are clustered at opposite sides of the helix.³ Positions Ser-457, Phe-459, Pro-463, Met-465, Thr-469 and Ile-472 are facing the lipid interface; thus, the location of these gain-of-function mutants is consistent with those of previously reported mutant nAChRs such as the Torpedo α M4 C418W and the *Mus musculus* α M3 C447W and L440W. In contrast, positions Val-464, Leu-467, Gly-468 and Phe-469 are facing the interior of

the protein. According to the nAChR structure, these positions are oriented toward crevices facing the M1 and M3 TMDs.³ These crevices allow for the accommodation of the bulky Trp side chain and the observed gain-of-functions of these mutations could be due to interactions of these positions with the neighboring TMDs during channel gating, leading to a stabilization of the open-channel state. In addition, the changes in periodicity and localization of residues in the helical net diagrams of the closed-and open-channel states could indicate a structural transition between helix types in this segment of the TMD, suggesting that this part of the TMD has a high propensity for helical distortions. This type of helical transition has been previously reported for the δ M3 TMD of the nAChR.²⁶

The existence of a Thr-Pro motif on the δ M4 TMD suggests a model in which, during the transition between the closed- and open-channel states, a dynamic molecular hinge formed at positions 462–463 experiences a hinge-bending motion that tilts the helical structure while combined with a spring-like motion of the two helical domains that flank the Thr-Pro motif. This molecular hinge could have a structural role by contributing to the overall architecture of the TMD and to the proper positioning of key amino acid side chains in the transmembrane region.^{77,78} Pro-containing sequence motifs in transmembrane helices have emerged as key elements in possible conformational “switches” underlying gating of some channels.⁷² A molecular hinge located in the lipid-protein interface could have a functional role by stabilizing nAChR structure and function by preserving motifs that are known or presumed to be essential for channel gating through direct interactions with cholesterol in the protein-lipid interface. The nAChR has been shown to contain internal sites capable of containing cholesterol whose occupation stabilizes protein structure and regulate function, and molecular dynamics simulations have identified residues Phe-471, Ile-472 and Met-475 as being involved in nAChR-cholesterol interactions.⁷⁹ The motions associated to the proposed molecular hinge could help position these key residues at an appropriate distance for protein-cholesterol interactions.

The structural model of the closed-channel state of the muscle-type nAChR is known to a 4.0 Å resolution.³ This model defines the secondary structure of the TMDs of all subunits as perfect α -helices. However, many transmembrane helices are not ideal straight helices.⁸⁰ More than 70% of helices in proteins are curved, bent or contain other non- α -helical structures such as kinks, 3_{10} -helices and π -bulges.^{81,82} This is particularly the case for polytopic transmembrane proteins, such as ion channels and G-protein-coupled receptors. Atomic resolution data from the nAChR TMDs in the closed- and open-channel states is still unavailable. Therefore, some uncertainty remains as to the exact positioning of the amino acid side chains along the TMDs and to the finer structural details such as bends and kinks. In this regard, the present study revealed distortions, including a sharp bending point, along the helical structure of the δ M4 TMD that are not present on current models of the nAChR. The recent high-resolution structure of the GluCl Cys-loop receptor reveals a highly bent TMD4 in each subunit, an observation that is consistent with our assessment of the secondary structure of the nAChR

δ M4 TMD.⁹ In addition, the present functional data emphasizes the role played by lipid-exposed domains on the gating machinery of the nAChR, as the δ M4 TMD seems to play an important role in the mechanism of channel gating of the Torpedo nAChR. Finally, we hypothesize a model for the secondary structure of the nAChR δ M4 TMD that includes a molecular hinge and discuss its possible functional implications. Further studies are needed to corroborate the proposed model's accuracy and potential role in nAChR channel gating.

Materials and Methods

Mutagenesis procedures. The coding regions of all *Torpedo californica* nAChR subunits were sub-cloned into the EcoRI/Hind III site of the pGEM-3Zf(-) vector under the SP6 promoter (Promega). Seventeen mutations along the core of the *Torpedo californica* nAChR δ M4 transmembrane domain (Leu-456 to Ile-472) were engineered with the QuikChangeTM site directed mutagenesis kit (Stratagene). Oligonucleotide primers were generated with the tryptophan codon (TGG) instead of the wild type (WT) codon at the desired position (Invitrogen). The successful inclusion of mutations was confirmed by DNA sequence analysis performed at the DNA Sequencing Facility in the section of Evolution and Ecology, University of California, Davis, CA. All pGEM-3Zf(-) vectors containing the coding region of the Torpedo nAChR subunits were linearized using the SmaI site and the digested products were purified with the Wizard[®] DNA Clean-Up System (Promega). Torpedo nAChR cRNA transcripts were produced with the SP6 mMessage mMachine Kit (Ambion). Transcripts were extracted once with an equal volume of phenol:chloroform:isoamyl alcohol (25:24:1, pH 4.5) and once with an equal volume of chloroform:isoamyl alcohol (24:1, pH 4.5), precipitated with 2.5 volumes of 100% ethanol at -20°C, dried and resuspended in RNase-free H₂O. The integrity and quantity of each cRNA was verified by gel-electrophoresis, weight markers and spectrophotometry, respectively.

nAChR expression in *Xenopus laevis* oocytes. Stage V–VI oocytes were extracted from *Xenopus laevis* frogs in accordance with the guidelines of the University of Puerto Rico Institutional Animal Care and Use Committee. The oocytes were incubated in collagenase type IA (Sigma-Aldrich) and this treatment was followed by manual defolliculation to remove follicles. RNA transcripts (55 ng total cRNA/oocyte) of the *Torpedo californica* nAChR α , β , γ and δ (WT or mutant) subunits were microinjected at a 2:1:1:1 subunit stoichiometry. The cRNA mixtures were pressure injected using a positive displacement injector (Drummond Instruments). The injected oocytes were incubated at 19°C in ND-96 media [96 mM NaCl, 2 mM KCl, 1.8 mM CaCl₂, 1 mM MgCl₂, 5 mM *N*-(2-hydroxyethyl)piperazine-*N'*-2-ethanesulfonic acid (HEPES), 2.5 mM Na-pyruvate] supplemented with 400 μ g/mL bovine serum albumin (BSA), 50 μ g/mL gentamicin, 50 μ g/mL tetracycline and 0.5 mM theophylline. The incubation media was changed daily. Electrophysiology experiments were performed 3 d after cRNA injection.

Electrophysiological recordings. ACh-induced macroscopic currents were recorded using a GeneClamp 500B amplifier in a

two-electrode voltage clamp configuration (Axon Instruments) at room temperature. Electrodes were filled with 3 M KCl and had resistances <5 MΩ. Impaled oocytes were automatically perfused with MOR-2 buffer [115 mM NaCl, 2.5 mM KCl, 5 mM MgCl₂, 1 mM Na₂HPO₄, 5 mM HEPES and 0.2 mM CaCl₂ (pH 7.4)] at a rate of 30 mL/min using an eight-channel perfusion valve controller (VC-8; Warner Instruments). Membrane potential was held at -70 mV. Membrane currents were filtered at 20 Hz and digitized at 5 kHz using a DigiData 1322A interface (Axon Instruments), and data were acquired using Clampex 9.2 from the pClamp 9.2 software package (Axon Instruments). Concentration-Response curves were generated from macroscopic peak currents (*I*) obtained from six ACh concentrations (1, 3, 10, 30, 100 and 300 μM). Agonist application was performed for 4 sec. GraphPad Prism 4.0 (GraphPad Software Inc.) was used to perform a nonlinear regression fit with a sigmoidal concentration-response equation with variable slope:²³

$$I = I_{min} + \frac{I_{max} - I_{min}}{1 + 10^{((\text{Log}EC_{50} - \text{Log}[ACh]) * nH)}}$$

where *I* is the macroscopic current at a given ACh concentration; *I*_{max} and *I*_{min} are the maximum and the minimum current responses recorded; *EC*₅₀ is the ACh concentration required to achieve half of the maximum response; [*ACh*] is the concentration of acetylcholine and *nH* is the Hill coefficient, which represents the steepness of the concentration-response curve.

¹²⁵I-labeled α-bungarotoxin binding assays. ¹²⁵I-labeled α-bungarotoxin (¹²⁵I-labeled α-BgTx) binding assays (Perkin-Elmer Life and Analytical Sciences) were performed immediately after voltage clamp measurements for the same oocytes to determine nAChR expression levels in the plasmatic membrane. Oocytes were incubated in 20 nM ¹²⁵I-labeled α-BgTx, 10 mg/mL BSA, MOR-2 without EGTA, and in the absence of agonist at room temperature for 1.5 h. Non-injected oocytes were incubated under the same conditions to measure non-specific binding. Individual oocytes were washed with 25 mL of MOR-2 without EGTA to remove excess toxin. Calibration curves were used to determine ¹²⁵I-labeled α-BgTx binding sites in the plasmatic membrane (nAChR expression levels) of each oocyte and they were constructed by plotting radioactivity (counts/min) as a function of ¹²⁵I-labeled α-BgTx concentration (fmol). Radioactivity was measured using a 2470 Wizard² Automatic Gamma Counter (Perkin Elmer Life and Analytical Sciences).

Normalized macroscopic nAChR response. The normalized response (-nA/fmol) for each oocyte was assessed as the ratio of the macroscopic peak current (-nA) induced by a 300 μM ACh concentration to the ¹²⁵I-labeled α-BgTx binding sites (fmol) in the plasmatic membrane (nAChR expression levels).

Periodicity profiles. The number of residues per helical turn for the open- and closed-channel states was determined by periodicity profiles for the *EC*₅₀ for ACh activation and ¹²⁵I-labeled α-BgTx binding sites in the plasmatic membrane (nAChR expression levels), respectively. Periodicity profiles were plotted with the *EC*₅₀ for ACh activation or ¹²⁵I-labeled α-BgTx binding sites as a function of the substituted position along the δM4 transmembrane domain. The produced oscillation patterns were best fitted by a cubic spline function using GraphPad Prism 4.0 (GraphPad Software Inc., San Diego, CA). The number of residues per helical turn of the periodicity profiles was estimated as the number of amino acids between the adjacent maximum and minimum peaks. nAChR expression levels (fmol) for each mutant were standardized (*X*_{Standardized}) to the change in amino acid volume (Å³) caused by the tryptophan substitution at that position (fmol/Å³):²⁴

$$X_{\text{Standardized}} = \frac{X_{\text{Mutant}}}{(V_{\text{Trp}} - V_{\text{WT}})}$$

where *X*_{Mutant} is the δM4 mutant nAChR expression level, and *V*_{Trp} and *V*_{WT} are the volumes of tryptophan and of the original residue, respectively. Amino acid volumes were taken from crystallographic studies.⁸³

Helical net diagrams. Helical net diagrams were prepared as described previously in reference 24–26.

Statistical analysis. Error estimates for *EC*₅₀ values are expressed as the mean ± SEM and the 95% confidence intervals. All other error estimates are expressed as the mean ± SEM. Two-sample comparisons were made using an unpaired t-test with Welch's correction. For more than two groups, an ANOVA with a Dunnett's post-test analysis was performed (GraphPad Software Inc.). A two-tailed p value < 0.05 was considered significant.

Disclosure of Potential Conflicts of Interest

No potential conflicts of interest were disclosed.

Acknowledgements

This work was supported by NIH Grants 2RO1GM56371-12 and 2U54NS43011. Daniel Caballero-Rivera was sponsored by the Research Initiative for Scientific Enhancement (RISE) Program (NIH grant 2 R25 GM061151), the Puerto Rico Industrial Development Company (PRIDCO) and the UPR Golf Tournament Fellowship. Jessica Oyola-Cintrón was supported by the Research Initiative for Scientific Enhancement (RISE) Program (NIH grant 2 R25 GM061151) and the Puerto Rico Industrial Development Company (PRIDCO).

Note

Supplemental materials may be found here:
www.landesbioscience.com/journals/channels/article/19540

References

- Corringer PJ, Le Novère N, Changeux JP. Nicotinic receptors at the amino acid level. *Annu Rev Pharmacol Toxicol* 2000; 40:431-58; PMID:10836143; <http://dx.doi.org/10.1146/annurev.pharmtox.40.1.431>.
- Karlin A. Emerging structure of the nicotinic acetylcholine receptors. *Nat Rev Neurosci* 2002; 3:102-14; PMID:11836518; <http://dx.doi.org/10.1038/nrn731>.
- Unwin N. Refined structure of the nicotinic acetylcholine receptor at 4 Å resolution. *J Mol Biol* 2005; 346:967-89; PMID:15701510; <http://dx.doi.org/10.1016/j.jmb.2004.12.031>.
- Kalamida D, Poulas K, Avramopoulou V, Fostieri E, Lagoumintzis G, Lazaridis K, et al. Muscle and neuronal nicotinic acetylcholine receptors. Structure, function and pathogenicity. *FEBS J* 2007; 274:3799-845; PMID:17651090; <http://dx.doi.org/10.1111/j.1742-4658.2007.05935.x>.
- Barrantes FJ. Structural basis for lipid modulation of nicotinic acetylcholine receptor function. *Brain Res Brain Res Rev* 2004; 47:71-95; PMID:15572164; <http://dx.doi.org/10.1016/j.brainresrev.2004.06.008>.
- Hilf RJ, Dutzler R. Structure of a potentially open state of a proton-activated pentameric ligand-gated ion channel. *Nature* 2009; 457:115-8; PMID:18987630; <http://dx.doi.org/10.1038/nature07461>.
- Bocquet N, Nury H, Baaden M, Le Poupon C, Changeux JP, Delarue M, et al. X-ray structure of a pentameric ligand-gated ion channel in an apparently open conformation. *Nature* 2009; 457:111-4; PMID:18987633; <http://dx.doi.org/10.1038/nature07462>.
- Hilf RJ, Dutzler R. X-ray structure of a prokaryotic pentameric ligand-gated ion channel. *Nature* 2008; 452:375-9; PMID:18322461; <http://dx.doi.org/10.1038/nature06717>.
- Hibbs RE, Gouaux E. Principles of activation and permeation in an anion-selective Cys-loop receptor. *Nature* 2011; 474:54-60; PMID:21572436; <http://dx.doi.org/10.1038/nature10139>.
- Miyazawa A, Fujiyoshi Y, Unwin N. Structure and gating mechanism of the acetylcholine receptor pore. *Nature* 2003; 423:949-55; PMID:12827192; <http://dx.doi.org/10.1038/nature01748>.
- Brejč K, van Dijk WJ, Klaassen RV, Schuurmans M, van Der Oost J, Smit AB, et al. Crystal structure of an ACh-binding protein reveals the ligand-binding domain of nicotinic receptors. *Nature* 2001; 411:269-76; PMID:11357122; <http://dx.doi.org/10.1038/35077011>.
- Dellisanti CD, Yao Y, Stroud JC, Wang ZZ, Chen L. Crystal structure of the extracellular domain of nAChR alpha1 bound to alpha-bungarotoxin at 1.94 Å resolution. *Nat Neurosci* 2007; 10:953-62; PMID:17643119; <http://dx.doi.org/10.1038/nn1942>.
- Blanton MP, Cohen JB. Mapping the lipid-exposed regions in the *Torpedo californica* nicotinic acetylcholine receptor. *Biochemistry* 1992; 31:3738-50; PMID:1567828; <http://dx.doi.org/10.1021/bi00130a003>.
- Blanton MP, Cohen JB. Identifying the lipid-protein interface of the *Torpedo* nicotinic acetylcholine receptor: secondary structure implications. *Biochemistry* 1994; 33:2859-72; PMID:8130199; <http://dx.doi.org/10.1021/bi00176a016>.
- Blanton MP, Dangott LJ, Raja SK, Lala AK, Cohen JB. Probing the structure of the nicotinic acetylcholine receptor ion channel with the uncharged photoactivatable compound -3H-diazofluorene. *J Biol Chem* 1998; 273:8659-68; PMID:9535841; <http://dx.doi.org/10.1074/jbc.273.15.8659>.
- Baenziger JE, Méthot N. Fourier transform infrared and hydrogen/deuterium exchange reveal an exchange-resistant core of α -helical peptide hydrogens in the nicotinic acetylcholine receptor. *J Biol Chem* 1995; 270:29129-37; PMID:7493938; <http://dx.doi.org/10.1074/jbc.270.49.29129>.
- Méthot N, Baenziger JE. Secondary structure of the exchange-resistant core from the nicotinic acetylcholine receptor probed directly by infrared spectroscopy and hydrogen/deuterium exchange. *Biochemistry* 1998; 37:14815-22; PMID:9778355; <http://dx.doi.org/10.1021/bi980848o>.
- Lugovskoy AA, Maslennikov IV, Utkin YN, Tsetlin VI, Cohen JB, Arseniev AS. Spatial structure of the M3 transmembrane segment of the nicotinic acetylcholine receptor alpha subunit. *Eur J Biochem* 1998; 255:455-61; PMID:9716388; <http://dx.doi.org/10.1046/j.1432-327.1998.2550455.x>.
- Tamamizu S, Guzmán GR, Santiago J, Rojas LV, McNamee MG, Lasalde-Dominicci JA. Functional effects of periodic tryptophan substitutions in the alpha M4 transmembrane domain of the *Torpedo californica* nicotinic acetylcholine receptor. *Biochemistry* 2000; 39:4666-73; PMID:10769122; <http://dx.doi.org/10.1021/bi992835w>.
- Guzmán GR, Santiago J, Ricardo A, Martí-Arbona R, Rojas LV, Lasalde-Dominicci JA. Tryptophan scanning mutagenesis in the alphaM3 transmembrane domain of the *Torpedo californica* acetylcholine receptor: functional and structural implications. *Biochemistry* 2003; 42:12243-50; PMID:14567686; <http://dx.doi.org/10.1021/bi034764d>.
- Santiago J, Guzmán GR, Torruellas K, Rojas LV, Lasalde-Dominicci JA. Tryptophan scanning mutagenesis in the TM3 domain of the *Torpedo californica* acetylcholine receptor beta subunit reveals an α -helical structure. *Biochemistry* 2004; 43:10064-70; PMID:15287734; <http://dx.doi.org/10.1021/bi0362368>.
- Navedo M, Nieves M, Rojas L, Lasalde-Dominicci JA. Tryptophan substitutions reveal the role of nicotinic acetylcholine receptor alpha-TM3 domain in channel gating: differences between *Torpedo* and muscle-type AChR. *Biochemistry* 2004; 43:78-84; PMID:14705933; <http://dx.doi.org/10.1021/bi0356496>.
- Ortiz-Acevedo A, Melendez M, Asseo AM, Biaggi N, Rojas LV, Lasalde-Dominicci JA. Tryptophan scanning mutagenesis of the gammaM4 transmembrane domain of the acetylcholine receptor from *Torpedo californica*. *J Biol Chem* 2004; 279:42250-7; PMID:15247226; <http://dx.doi.org/10.1074/jbc.M405132200>.
- Otero-Cruz JD, Báez-Pagán CA, Caraballo-González IM, Lasalde-Dominicci JA. Tryptophan-scanning mutagenesis in the alphaM3 transmembrane domain of the muscle-type acetylcholine receptor. A spring model revealed. *J Biol Chem* 2007; 282:9162-71; PMID:17242410; <http://dx.doi.org/10.1074/jbc.M607492200>.
- Díaz-De León R, Otero-Cruz JD, Torres-Núñez DA, Casiano A, Lasalde-Dominicci JA. Tryptophan scanning of the acetylcholine receptor's betaM4 transmembrane domain: decoding allosteric linkage at the lipid-protein interface with ion-channel gating. *Channels (Austin)* 2008; 2:439-48; PMID:19066450; <http://dx.doi.org/10.4161/chan.2.6.7130>.
- Caballero-Rivera D, Cruz-Nieves OA, Oyola-Cintrón J, Torres-Núñez DA, Otero-Cruz JD, Lasalde-Dominicci JA. Fourier transform coupled tryptophan scanning mutagenesis identifies a bending point on the lipid-exposed δ M3 transmembrane domain of the *Torpedo californica* nicotinic acetylcholine receptor. *Channels (Austin)* 2011; 5:345-56; PMID:21785268; <http://dx.doi.org/10.4161/chan.5.4.17082>.
- Choe S, Stevens CF, Sullivan JM. Three distinct structural environments of a transmembrane domain in the inwardly rectifying potassium channel ROMK1 defined by perturbation. *Proc Natl Acad Sci USA* 1995; 92:12046-9; PMID:8618841; <http://dx.doi.org/10.1073/pnas.92.26.12046>.
- Collins A, Chuang H, Jan YN, Jan LY. Scanning mutagenesis of the putative transmembrane segments of Kir2.1, an inward rectifier potassium channel. *Proc Natl Acad Sci USA* 1997; 94:5456-60; PMID:9144259; <http://dx.doi.org/10.1073/pnas.94.10.5456>.
- Cukras CA, Jeliakova I, Nichols CG. Structural and functional determinants of conserved lipid interaction domains of inward rectifying Kir6.2 channels. *J Gen Physiol* 2002; 119:581-91; PMID:12034765; <http://dx.doi.org/10.1085/jgp.20028562>.
- Li-Smerin Y, Hackos DH, Swartz KJ. A localized interaction surface for voltage-sensing domains on the pore domain of a K⁺ channel. *Neuron* 2000; 25:411-23; PMID:10719895; [http://dx.doi.org/10.1016/S0896-6273\(00\)80904-6](http://dx.doi.org/10.1016/S0896-6273(00)80904-6).
- Li-Smerin Y, Hackos DH, Swartz KJ. α -helical structural elements within the voltage-sensing domains of a K⁺ channel. *J Gen Physiol* 2000; 115:33-50; PMID:10613917; <http://dx.doi.org/10.1085/jgp.115.1.33>.
- Li-Smerin Y, Swartz KJ. Helical structure of the COOH terminus of S3 and its contribution to the gating modifier toxin receptor in voltage-gated ion channels. *J Gen Physiol* 2001; 117:205-18; PMID:11222625; <http://dx.doi.org/10.1085/jgp.117.3.205>.
- Irizarry SN, Kutluay E, Drews G, Hart SJ, Heginbotham L. Opening the KcsA K⁺ channel: tryptophan scanning and complementation analysis lead to mutants with altered gating. *Biochemistry* 2002; 41:13653-62; PMID:12427027; <http://dx.doi.org/10.1021/bi026393r>.
- Jenkins A, Andreasen A, Trudell JR, Harrison NL. Tryptophan scanning mutagenesis in TM4 of the GABA(A) receptor alpha1 subunit: implications for modulation by inhaled anesthetics and ion channel structure. *Neuropharmacology* 2002; 43:669-78; PMID:12367612; [http://dx.doi.org/10.1016/S0028-3908\(02\)00175-2](http://dx.doi.org/10.1016/S0028-3908(02)00175-2).
- Wang SY, Bonner K, Russell C, Wang GK. Tryptophan scanning of D1S6 and D4S6 C-termini in voltage-gated sodium channels. *Biophys J* 2003; 85:911-20; PMID:12885638; [http://dx.doi.org/10.1016/S0006-3495\(03\)74530-5](http://dx.doi.org/10.1016/S0006-3495(03)74530-5).
- Honse Y, Ren H, Lipsky RH, Peoples RW. Sites in the fourth membrane-associated domain regulate alcohol sensitivity of the NMDA receptor. *Neuropharmacology* 2004; 46:647-54; PMID:14996542; <http://dx.doi.org/10.1016/j.neuropharm.2003.11.006>.
- Silberberg SD, Chang TH, Swartz KJ. Secondary structure and gating rearrangements of transmembrane segments in rat P2X4 receptor channels. *J Gen Physiol* 2005; 125:347-59; PMID:15795310; <http://dx.doi.org/10.1085/jgp.200409221>.
- Powl AM, Wright JN, East JM, Lee AG. Identification of the hydrophobic thickness of a membrane protein using fluorescence spectroscopy: studies with the mechanosensitive channel MscL. *Biochemistry* 2005; 44:5713-21; PMID:15823029; <http://dx.doi.org/10.1021/bi047338g>.
- Cordes FS, Bright JN, Sansom MS. Proline-induced distortions of transmembrane helices. *J Mol Biol* 2002; 323:951-60; PMID:12417206; [http://dx.doi.org/10.1016/S0022-2836\(02\)01006-9](http://dx.doi.org/10.1016/S0022-2836(02)01006-9).
- Woolfson DN, Williams DH. The influence of proline residues on α -helical structure. *FEBS Lett* 1990; 277:185-8; PMID:2269352; [http://dx.doi.org/10.1016/0014-5793\(90\)80839-B](http://dx.doi.org/10.1016/0014-5793(90)80839-B).
- Deupi X, Olivella M, Govaerts C, Ballesteros JA, Campillo M, Pardo L. Ser and Thr residues modulate the conformation of pro-kinked transmembrane alpha-helices. *Biophys J* 2004; 86:105-15; PMID:14695254; [http://dx.doi.org/10.1016/S0006-3495\(04\)74088-6](http://dx.doi.org/10.1016/S0006-3495(04)74088-6).
- McGregor MJ, Islam SA, Sternberg MJ. Analysis of the relationship between side-chain conformation and secondary structure in globular proteins. *J Mol Biol* 1987; 198:295-310; PMID:3430610; [http://dx.doi.org/10.1016/0022-2836\(87\)90314-7](http://dx.doi.org/10.1016/0022-2836(87)90314-7).
- Okamoto T, Schlegel A, Scherer PE, Lisanti MP. Caveolins, a family of scaffolding proteins for organizing "preassembled signaling complexes" at the plasma membrane. *J Biol Chem* 1998; 273:5419-22; PMID:9488658; <http://dx.doi.org/10.1074/jbc.273.10.5419>.

44. Couet J, Li S, Okamoto T, Ikezu T, Lisanti MP. Identification of peptide and protein ligands for the caveolin-scaffolding domain. Implications for the interaction of caveolin with caveolae-associated proteins. *J Biol Chem* 1997; 272:6525-33; PMID:9045678; <http://dx.doi.org/10.1074/jbc.272.10.6525>.
45. Carman CV, Lisanti MP, Benovic JL. Regulation of G protein-coupled receptor kinases by caveolin. *J Biol Chem* 1999; 274:8858-64; PMID:10085129; <http://dx.doi.org/10.1074/jbc.274.13.8858>.
46. Báez-Pagán CA, Martínez-Ortiz Y, Otero-Cruz JD, Salgado-Villanueva IK, Velázquez G, Ortiz-Acevedo A, et al. Potential role of caveolin-1-positive domains in the regulation of the acetylcholine receptor's activatable pool: implications in the pathogenesis of a novel congenital myasthenic syndrome. *Channels (Austin)* 2008; 2:180-90; PMID:18836288; <http://dx.doi.org/10.4161/chan.2.3.6155>.
47. Cruz-Martín A, Mercado JL, Rojas LV, McNamee MG, Lasalde-Dominicci JA. Tryptophan substitutions at lipid-exposed positions of the gamma M3 transmembrane domain increase the macroscopic ionic current response of the *Torpedo californica* nicotinic acetylcholine receptor. *J Membr Biol* 2001; 183:61-70; PMID:11547353; <http://dx.doi.org/10.1007/s00232-001-0051-z>.
48. Lasalde JA, Tamamizu S, Butler DH, Vibat CR, Hung B, McNamee MG. Tryptophan substitutions at the lipid-exposed transmembrane segment M4 of *Torpedo californica* acetylcholine receptor govern channel gating. *Biochemistry* 1996; 35:14139-48; PMID:8916899; <http://dx.doi.org/10.1021/bi961583l>.
49. Lee YH, Li L, Lasalde J, Rojas L, McNamee M, Ortiz-Miranda SI, et al. Mutations in the M4 domain of *Torpedo californica* acetylcholine receptor dramatically alter ion channel function. *Biophys J* 1994; 66:646-53; PMID:7516721; [http://dx.doi.org/10.1016/S0006-3495\(94\)80838-0](http://dx.doi.org/10.1016/S0006-3495(94)80838-0).
50. Li L, Lee YH, Pappone P, Palma A, McNamee MG. Site-specific mutations of nicotinic acetylcholine receptor at the lipid-protein interface dramatically alter ion channel gating. *Biophys J* 1992; 62:61-3; PMID:1600100; [http://dx.doi.org/10.1016/S0006-3495\(92\)81779-4](http://dx.doi.org/10.1016/S0006-3495(92)81779-4).
51. Li L, Schuchard M, Palma A, Pradier L, McNamee MG. Functional role of the cysteine 451 thiol group in the M4 helix of the gamma subunit of *Torpedo californica* acetylcholine receptor. *Biochemistry* 1990; 29:5428-36; PMID:1696834; <http://dx.doi.org/10.1021/bi00475a003>.
52. Ortiz-Miranda SI, Lasalde JA, Pappone PA, McNamee MG. Mutations in the M4 domain of the *Torpedo californica* nicotinic acetylcholine receptor alter channel opening and closing. *J Membr Biol* 1997; 158:17-30; PMID:9211718; <http://dx.doi.org/10.1007/s002329900240>.
53. Tamamizu S, Lee Y, Hung B, McNamee MG, Lasalde-Dominicci JA. Alteration in ion channel function of mouse nicotinic acetylcholine receptor by mutations in the M4 transmembrane domain. *J Membr Biol* 1999; 170:157-64; PMID:10430659; <http://dx.doi.org/10.1007/s002329900545>.
54. Santiago J, Guzmán GR, Rojas LV, Martí R, Asmar-Rovira GA, Santana LF, et al. Probing the effects of membrane cholesterol in the *Torpedo californica* acetylcholine receptor and the novel lipid-exposed mutation alpha C418W in *Xenopus* oocytes. *J Biol Chem* 2001; 276:46523-32; PMID:11567020; <http://dx.doi.org/10.1074/jbc.M104563200>.
55. Shen XM, Deymeer F, Sine SM, Engel AG. Slow-channel mutation in acetylcholine receptor alphaM4 domain and its efficient knockdown. *Ann Neurol* 2006; 60:128-36; PMID:16685696; <http://dx.doi.org/10.1002/ana.20861>.
56. Ri Y, Ballesteros JA, Abrams CK, Oh S, Verselis VK, Weinstein H, et al. The role of a conserved proline residue in mediating conformational changes associated with voltage gating of Cx32 gap junctions. *Biophys J* 1999; 76:2887-98; PMID:10354417; [http://dx.doi.org/10.1016/S0006-3495\(99\)77444-8](http://dx.doi.org/10.1016/S0006-3495(99)77444-8).
57. Luecke H, Schobert B, Richter HT, Carttailler JP, Lanyi JK. Structure of bacteriorhodopsin at 1.55 Å resolution. *J Mol Biol* 1999; 291:899-911; PMID:10452895; <http://dx.doi.org/10.1006/jmbi.1999.3027>.
58. Gether U. Uncovering molecular mechanisms involved in activation of G protein-coupled receptors. *Endocr Rev* 2000; 21:90-113; PMID:10696571; <http://dx.doi.org/10.1210/er.21.1.90>.
59. Sansom MS, Weinstein H. Hinges, swivels and switches: the role of prolines in signalling via transmembrane alpha-helices. *Trends Pharmacol Sci* 2000; 21:445-51; PMID:11121576; [http://dx.doi.org/10.1016/S0165-6147\(00\)01553-4](http://dx.doi.org/10.1016/S0165-6147(00)01553-4).
60. Deupi X, Olivella M, Sanz A, Dölker N, Campillo M, Pardo L. Influence of the g- conformation of Ser and Thr on the structure of transmembrane helices. *J Struct Biol* 2010; 169:116-23; PMID:19766191; <http://dx.doi.org/10.1016/j.jsb.2009.09.009>.
61. Nilsson I, Säaf A, Whitley P, Gafvelin G, Waller C, von Heijne G. Proline-induced disruption of a transmembrane alpha-helix in its natural environment. *J Mol Biol* 1998; 284:1165-75; PMID:9837734; <http://dx.doi.org/10.1006/jmbi.1998.2217>.
62. Zhu F, Hummer G. Gating transition of pentameric ligand-gated ion channels. *Biophys J* 2009; 97:2456-63; PMID:19883588; <http://dx.doi.org/10.1016/j.bpj.2009.08.020>.
63. Mitra A, Bailey TD, Auerbach AL. Structural dynamics of the M4 transmembrane segment during acetylcholine receptor gating. *Structure* 2004; 12:1909-18; PMID:15458639; <http://dx.doi.org/10.1016/j.str.2004.08.004>.
64. Bouzat C, Barrantes F, Sine S. Nicotinic receptor fourth transmembrane domain: hydrogen bonding by conserved threonine contributes to channel gating kinetics. *J Gen Physiol* 2000; 115:663-72; PMID:10779322; <http://dx.doi.org/10.1085/jgp.115.5.663>.
65. Bouzat C, Gumilar F, del Carmen Esandi M, Sine SM. Subunit-selective contribution to channel gating of the M4 domain of the nicotinic receptor. *Biophys J* 2002; 82:1920-9; PMID:11916850; [http://dx.doi.org/10.1016/S0006-3495\(02\)75541-0](http://dx.doi.org/10.1016/S0006-3495(02)75541-0).
66. Sansom MS. Structure and function of channel-forming peptides. *Q Rev Biophys* 1993; 26:365-421; PMID:7520180; <http://dx.doi.org/10.1017/S0033583500002833>.
67. Kerr ID, Son HS, Sankaramakrishnan R, Sansom MS. Molecular dynamics simulations of isolated transmembrane helices of potassium channels. *Biopolymers* 1996; 39:503-15; PMID:8837517; [http://dx.doi.org/10.1002/\(SICI\)1097-0282\(199610\)39:4<503::AID-BIP3>3.3.CO;2-5](http://dx.doi.org/10.1002/(SICI)1097-0282(199610)39:4<503::AID-BIP3>3.3.CO;2-5).
68. Maduke M, Miller C, Mindell JA. A decade of CLC chloride channels: structure, mechanism and many unsettled questions. *Annu Rev Biophys Biomol Struct* 2000; 29:411-38; PMID:10940254; <http://dx.doi.org/10.1146/annurev.biophys.29.1.411>.
69. Unwin N. Acetylcholine receptor channel imaged in the open state. *Nature* 1995; 373:37-43; PMID:7800037; <http://dx.doi.org/10.1038/373037a0>.
70. Unwin N. Nicotinic acetylcholine receptor at 9 Å resolution. *J Mol Biol* 1993; 229:1101-24; PMID:8445638; <http://dx.doi.org/10.1111/j.1399-3011.1992.tb01595.x>.
71. Sankaramakrishnan R, Vishveshwara S. Geometry of proline-containing alpha-helices in proteins. *Int J Pept Protein Res* 1992; 39:356-63; PMID:1428525; <http://dx.doi.org/10.1111/j.1399-3011.1992.tb01595.x>.
72. Tieleman DP, Shrivastava IH, Ulmschneider MR, Sansom MS. Proline-induced hinges in transmembrane helices: possible roles in ion channel gating. *Proteins* 2001; 44:63-72; PMID:11391769; <http://dx.doi.org/10.1002/prot.1073>.
73. Sankaramakrishnan R, Vishveshwara S. Characterization of proline-containing alpha-helix (helix F model of bacteriorhodopsin) by molecular dynamics studies. *Proteins* 1993; 15:26-41; PMID:8451238; <http://dx.doi.org/10.1002/prot.340150105>.
74. Cha A, Snyder GE, Selvin PR, Bezanilla F. Atomic scale movement of the voltage-sensing region in a potassium channel measured via spectroscopy. *Nature* 1999; 402:809-13; PMID:10617201; <http://dx.doi.org/10.1038/45552>.
75. Glauner KS, Mannuzzu LM, Gandhi CS, Isacoff EY. Spectroscopic mapping of voltage sensor movement in the Shaker potassium channel. *Nature* 1999; 402:813-7; PMID:10617202; <http://dx.doi.org/10.1038/45561>.
76. Xu Y, Barrantes FJ, Luo X, Chen K, Shen J, Jiang H. Conformational dynamics of the nicotinic acetylcholine receptor channel: a 35-ns molecular dynamics simulation study. *J Am Chem Soc* 2005; 127:1291-9; PMID:15669869; <http://dx.doi.org/10.1021/ja044577i>.
77. Brandl CJ, Deber CM. Hypothesis about the function of membrane-buried proline residues in transport proteins. *Proc Natl Acad Sci USA* 1986; 83:917-21; PMID:3456574; <http://dx.doi.org/10.1073/pnas.83.4.917>.
78. Williams KA, Deber CM. Proline residues in transmembrane helices: structural or dynamic role? *Biochemistry* 1991; 30:8919-23; PMID:1892808; <http://dx.doi.org/10.1021/bi00101a001>.
79. Brannigan G, Hémin J, Law R, Eckenhoff R, Klein ML. Embedded cholesterol in the nicotinic acetylcholine receptor. *Proc Natl Acad Sci USA* 2008; 105:14418-23; PMID:18768796; <http://dx.doi.org/10.1073/pnas.0803029105>.
80. Yohannan S, Faham S, Yang D, Whitelegge JP, Bowie JU. The evolution of transmembrane helix kinks and the structural diversity of G protein-coupled receptors. *Proc Natl Acad Sci USA* 2004; 101:959-63; PMID:14732697; <http://dx.doi.org/10.1073/pnas.0306077101>.
81. Bansal M, Kumar S, Velavan R. HELANAL: a program to characterize helix geometry in proteins. *J Biomol Struct Dyn* 2000; 17:811-9; PMID:10798526.
82. Barlow DJ, Thornton JM. Helix geometry in proteins. *J Mol Biol* 1988; 201:601-19; PMID:3418712; [http://dx.doi.org/10.1016/0022-2836\(88\)90641-9](http://dx.doi.org/10.1016/0022-2836(88)90641-9).
83. Chothia C. Structural invariants in protein folding. *Nature* 1975; 254:304-8; PMID:1118010; <http://dx.doi.org/10.1038/254304a0>.